ACS APPLIED MATERIALS & INTERFACES

Research Article

www.acsami.org

Folded Elastic Strip-Based Triboelectric Nanogenerator for Harvesting Human Motion Energy for Multiple Applications

Yue Kang,[†,‡] Bo Wang,[†,§] Shuge Dai,[†] Guanlin Liu,[†] Yanping Pu,[‡] and Chenguo Hu*[,†]

[†]Department of Applied Physics, Chongqing University, Chongqing 400044, P. R. China

[‡]School of Public Affairs, Chongqing University, Chongqing 400044, P. R. China

[§]College of Materials Science and Engineering, Chongqing University, Chongqing 400044, P. R. China

Supporting Information

ABSTRACT: A folded elastic strip-based triboelectric nanogenerator (FS-TENG) made from two folded double-layer elastic strips of Al/PET and PTFE/PET can achieve multiple functions by low frequency mechanical motion. A single FS-TENG with strip width of 3 cm and length of 27 cm can generate a maximum output current, open-circuit voltage, and peak power of 55 μA, 840 V, and 7.33 mW at deformation frequency of 4 Hz with amplitude of 2.5 cm, respectively. This FS-TENG can work as a weight sensor due to its good elasticity. An integrated generator assembled by four FS-TENGs (IFS-TENG) can harvest the energy of human motion like flapping hands and walking steps. In addition, the IFS-TENG combined with electromagnetically induced electricity can achieve a completely self-driven doorbell with flashing lights. Moreover, a box-like generator integrated by four IFS-TENGs inside can work in horizontal or random motion modes and can be improved to harvest energy in all directions. This work promotes the research of completely self-driven systems and energy harvesting of human motion for applications in our daily life.

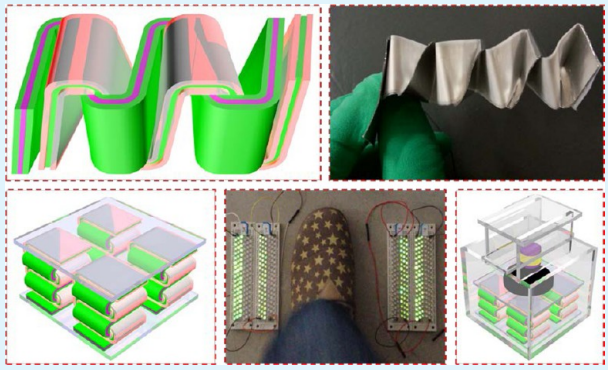

KEYWORDS: *folded elastic strip, nanogenerator, human motion, self-driven, doorbell*

1. INTRODUCTION

Since nanogenerators were first reported in 2006, they have attracted extensive interest throughout the world because they can harvest different energies by using different nanomaterials. Many types of nanogenerators have been designed and fabricated in recent years. In general, they can be classified into three kinds, namely, piezoelectric nanogenerators,[1−3] pyroelectric nanogenerators,[4−6] and triboelectric nanogenerators.[7−10] Among these, triboelectric nanogenerators (TENGs) are expected to be the most promising and valuable ones due to their universality, multifunction, and higher conversion efficiency. They can harvest almost all mechanical energy in the ambient including vibration,[11,12] rotation,[13,14] human motion,[15,16] and airflow.[17,18] On the basis of the triboelectrification effect and electrostatic induction effect[19] between two friction materials with opposite charges, TENGs convert the mechanical energy into electricity, achieving powering the mobile electronic devices.

To generate electricity, friction materials must contact and separate alternatively to form electron flows. According to different contact types, TENGs can work in vertical mode,[20,21] horizontal sliding mode,[22,23] and rotary mode.[24,25] In vertical mode, one triboelectric material must move up and down in order to contact/separate with/from the another one. In the ambient, low frequency mechanical energy exists everywhere, which can be used to drive a TENG to work. Most of the previous TENGs are used to harvest mechanical energy in one direction or in high frequency, or to work in one mode, which limits their applications. To broaden the applications, TENGs should be designed to have multifunctions.

Herein, we have demonstrated a folded elastic strip-based triboelectric nanogenerator (FS-TENG) for harvesting low frequency human motion energy and for a self-powered weight sensor and a buzzer bell. A single FS-TENG can produce an open-circuit voltage of about 840 V, maximum current of about 55 μA, and output power of 7.33 mW at 4 Hz. Meanwhile, the FS-TENG can be used as a weight sensor to detect different weights. The FS-TENGs made from different widths and lengths of the elastic strip, and at different frequencies and with displacement amplitudes, have been investigated. The integrated FS-TENG of four single units with size 6 cm × 6 cm × 3 cm can light 352 light-emitting diodes (LEDs) alternatively by hand or by foot. By introducing electromagnetic induction, the output performance of the FS-TENG is significantly enhanced, which can power a buzzer bell to alarm without other electrical power, working as a doorbell indicator. Being fixed on the inner

Received: July 23, 2015
Accepted: August 25, 2015
Published: August 25, 2015

DOI: 10.1021/acsami.5b06675
ACS Appl. Mater. Interfaces 2015, 7, 20469−20476

walls of an acrylic box, the box-like FS-TENG can harvest horizontal sliding (X axis and Y axis) energy and rotary energy simultaneously. Compared with the previous TENGs,[16,26] the electrodes of FS-TENG are integral and crosswise folded which is easily assembled. Also, this type of FS-TENG has multifunctions that could be used to detect weight, to illuminate shoes, and to power a doorbell in our daily life.

2. EXPERIMENTAL SECTION

2.1. Fabrication of a Single FS-TENG. A single FS-TENG is made of two parts. Part one consists of two pieces of PTFE strips with width of w cm (w = 1, 2, and 3) and length of l cm (l = 15, 21, 27), and a piece of aluminum foil with width of (w − 0.2) cm and length of l cm. Then, PTFE strips are attached to the surfaces of a narrow Al foil to form electrode A. Part two consists of two pieces of Al foil and a piece of polyethylene terephthalate (PET) film with the same width of w cm and length of l cm. Similarly, two Al foil strips are attached to the surface of PET film to form electrode B. In order to promote the output performance of FS-TENG, the PTFE strips are treated by surface inductively coupled plasma reactive ion etching to increase their nanostructure roughness. Also, the Al foils are etched by dilute sulfuric acid (0.02 M). Then, the prepared two parts are crosswise folded alternately to form the FS-TENG as is shown in Figure 1 and Figure S1.

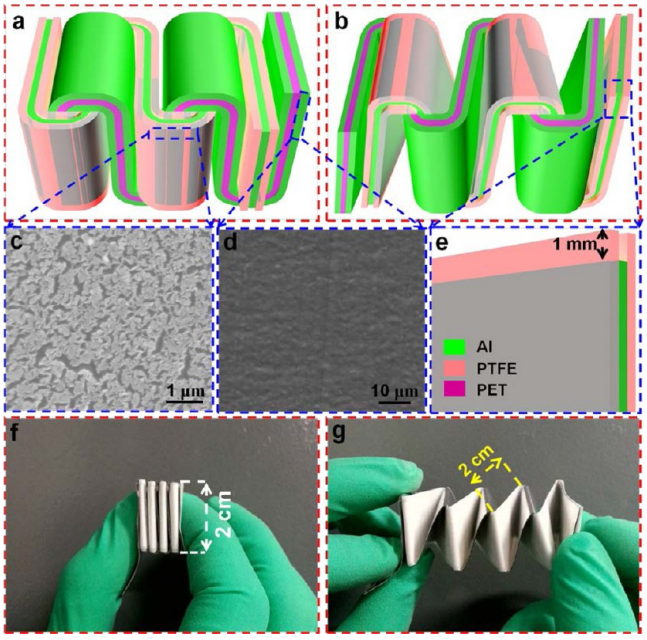

Figure 1. Schematic diagrams of the FS-TENG when pressed (a) and released (b), the SEM images of the surface of PTFE (c) and Al electrode (d), the magnified drawing of the end of part one (e), and digital photographs of the FS-TENG with width of 2 cm at pressure (f) and release (g) states, respectively.

2.2. Fabrication of an Integrated FS-TENG. Four FS-TENGs are attached to the four corners of an acrylic plate with size 6 cm × 6 cm. Another acrylic plate with the same size is fixed on the top of the integrated FS-TENG. The fabricated device has a total size of 6 cm × 6 cm × 3 cm. To realize the application in a doorbell, an acrylic box with a size of 7 cm × 7 cm × 7 cm is also made.

2.3. Fabrication of a Box FS-TENG. Two integrated FS-TENGs with 4 single units are attached to two inner opposite walls of an acrylic box with a size 10 cm × 10 cm × 10 cm. Another two integrated FS-TENGs with 2 single units are attached to the other two opposite walls. Then, two PTFE balls, one on top of the other, are placed in the cavity formed by these four integrated FS-TENGs. These two balls can simultaneously move forward/backward, left/right, or roll inside the box.

2.4. Fabrication of Self-Powered Doorbell. An iron core (silicon steel) wound by a Cu wire with the cycle number of 2000 to form a coil is fixed on an acrylic plate with size of 3 cm × 7 cm, which is mounted on the top of the acrylic box. The Cu coil works as the electric circuit for the collection of electromagnetic induced electricity. Besides, a $Nd_2Fe_{14}B$ permanent magnet with a radius of 2.5 cm and a height of 5 mm is attached on the movable acrylic plate of the integrated FS-TENG, on which a plate supported by two vertical acrylic plates is used to drive the integrated FS-TENG to work and to conduct contact/separation between the magnet and Cu coil by external force.

2.5. Characterization of FS-TENGs. The output currents of the FS-TENGs were measured using a standard low noise current preamplifier (Model SR570) and a data acquisition card (NI PCI-6259). The output voltages were measured with Keithley 6514.

3. RESULTS AND DISCUSSION

The fabrication process and the structure of the FS-TENG are shown in Figure 1 and Figure S1 (Supporting Information). Figure 1a,b shows the schematic diagrams of the FS-TENG when pressed and released, respectively. Figure 1c and Figure S2 illustrate the surface morphology of the PTFE strips treated by ion etching, which reveals a nanostructured roughness. The surface morphology of the Al foils treated by chemical etching is shown in Figure 1d. The detailed etching and corrosion processes are given in Supporting Information (page S-17). Figure 1e shows the magnified structure in Figure 1b, from which we can find that the width of the Al foil is 1 mm narrower than that of the PTFE strips, by which the contact (short-circuit) of electrode A in part one with electrode B in part two can be effectively avoided. Figure 1f,g shows the digital photographs of the FS-TENG with strip width of 2 cm under pressing and release, respectively, which shows perfect elasticity.

Figure 2 displays the working principle of the FS-TENG. When a force is applied to the ends of the FS-TENG, the PTFE strips in part one fully contact the Al foil in part two, which causes negative charges on the surfaces of the PTFE strips and

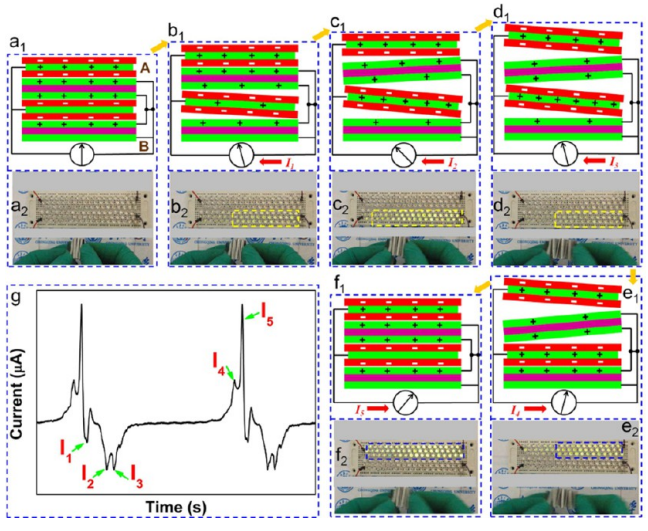

Figure 2. Working principle of the FS-TENG. The charge distributions and current signals at initial (a), intermediate (b, c), and final (d) stages when released, and the charge distributions and current signals when pressed (e, f). The output current peaks at different stages (g).

DOI: 10.1021/acsami.5b06675
ACS Appl. Mater. Interfaces 2015, 7, 20469−20476

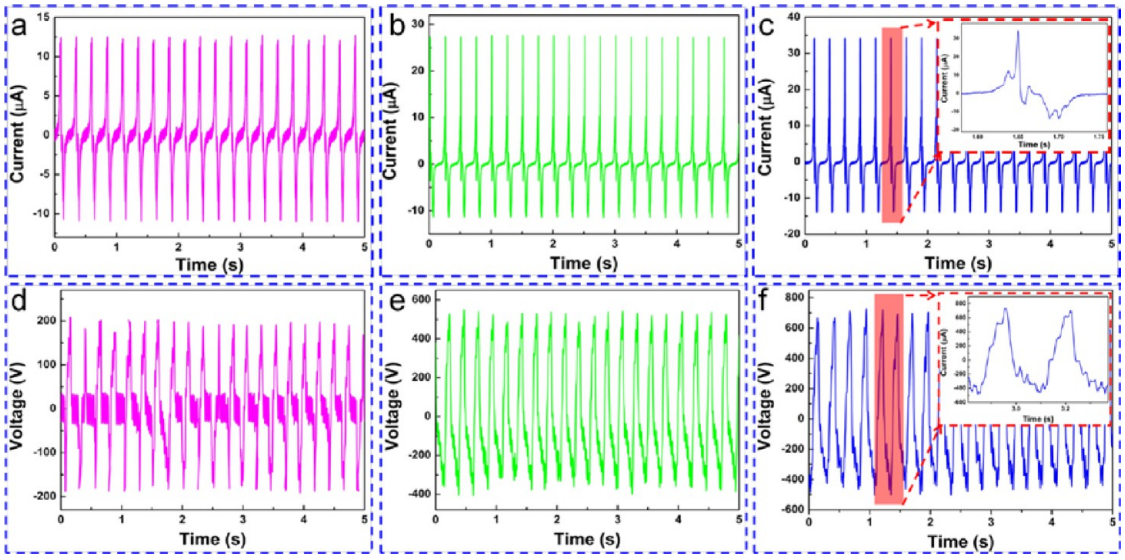

Figure 3. Output currents and voltages of the FS-TENGs with different widths of 1 cm (a, d), 2 cm (b, e), and 3 cm (c, f), respectively. The insets are the enlarged image of the selected peaks.

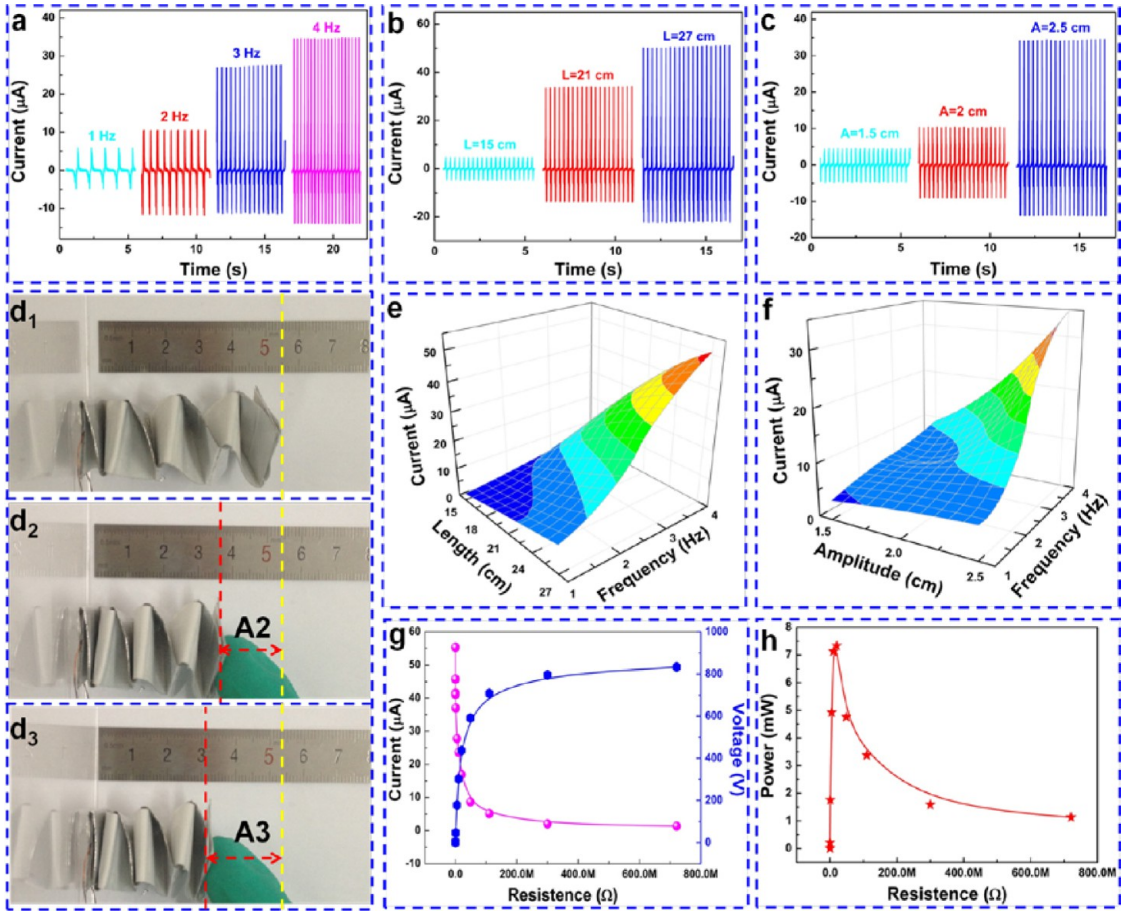

Figure 4. Output current change under different deformation frequencies (a), lengths of the strips (b), and deformation amplitudes (c). The optical images of the FS-TENG with different deformation amplitudes (d_1–d_3). The three-dimensional surface maps of the output current versus length of the strips and deformation frequency (e), and deformation amplitude and frequency (f). The output current and open-circuit voltage (g), and output power (h) under different external resistances.

positive charges on the Al foil (Figure 2a_1).[27] Due to electrostatic equilibrium, no output signal is detected, which can be verified by the unlit LEDs (Figure 2a_2). When the applied force is gradually released, the two parts begin to separate from the first to the third contact surfaces in turn due to the elasticity of the folded PTFE and PET strips. The induced charges on electrode B decrease while the charges on electrode A increase, which generates a current (I_1, I_2, and I_3)

DOI: 10.1021/acsami.5b06675
ACS Appl. Mater. Interfaces 2015, 7, 20469−20476

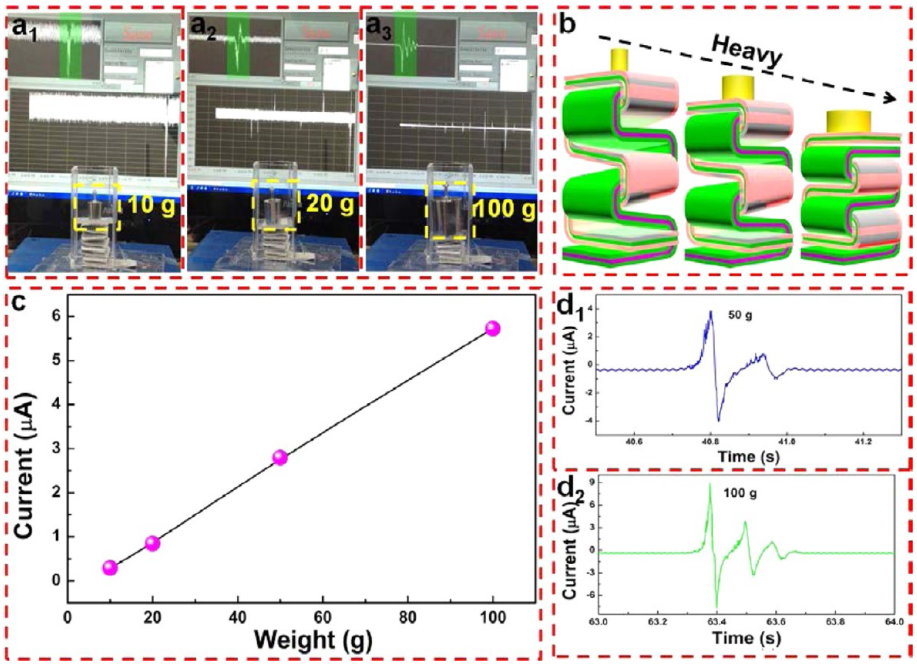

Figure 5. Digital photographs of the compressed FS-TENG under different weights and their output signals (a_1−a_3), the schematic diagram of the weight sensor (b), the output current signals under different weights (c), and the output current values under weights of 50 g (d_1) and 100 g (d_2), respectively.

flowing from electrode B to A in external circuit (Figure 2b_1,c_1,d_1), and the output current can be monitored by the lighted LEDs (Figure 2b_2,c_2,d_2). Once the external force is applied, the FS-TENG begins to shrink, and the separated surfaces begin to contact from the third to the first layers until they fully contact, as shown in Figure 2e_1,f_1. The induced charges on electrode A begin to flow back to electrode B, which generates a current (I_4 and I_5) flowing from electrode A to B (Figure 2e_1,f_1,g), and the output current can be monitored by the lighted LEDs (Figure 2e_1,f_1). The output current of the two working cycles can be seen in Figure 2g, in which the peak currents match well with I_1−I_5 in Figure 2b_1−f_1.

The output performances of the FS-TENG with different widths are investigated. As is shown in Figure 3, the output current of the FS-TENG with a width of 1, 2, and 3 cm can reach about 12.8, 28.5, and 34.6 μA, respectively (Figure 3a−c). As the width of PTFE strips and Al foils increases, the effective frication areas are enlarged. More induced charges are transferred during the contact and separation processes, which subsequently generate higher output current. Figure 3d−f depicts the corresponding open-circuit voltages of these three FS-TENGs. Just as the output currents do, the open-circuit voltages increase with an increase in width. The maximum open-circuit voltage with a width of 3 cm is about 740 V. The lengths of strips for these three FS-TENGs are all 21 cm, and the deformation frequency is 4 Hz.

Another vital factor that influences the output performance of the FS-TENG is the deformation frequency. Figure 4a shows the dependence of the output current on the deformation frequency from 1 to 4 Hz, where the output current increases from 5.91 μA at 1 Hz to 34.7 μA at 4 Hz, exhibiting an obvious increasing trend with the higher frequency. Since the total amount of the transferred charges keeps constant in the same conditions in a cycle,[28] the periods reduce with an increase in the deformation frequency, which leads to a higher output current due to a higher rate of charge transfer, according to eq 1.

$$I = \frac{dQ}{dt} = \frac{S d\sigma}{dt} \quad (1)$$

Here the dQ is the charge transfer quantity on the electrode within dt time (here in one period), and σ is charge density on the electrode surface, indicating I is proportional to electrode area S. The width and length of the electrodes under this condition are chosen to be 3 and 21 cm, respectively. Figure S3 shows the dependence of the output currents of the FS-TENGs on the widths of 1 and 2 cm at frequencies 1−4 Hz. The output performance of the FS-TENG changes with the change in the strip length. As is shown in Figure 4b, the output current of the FS-TENG with strip lengths of 15, 21, and 27 cm is about 4.7, 34.7, and 50.9 μA, respectively, with strip width of 3 cm at deformation frequency of 4 Hz. According to eq 1, the output current is proportional to S. The electrode area is enlarged with an increase in the length of the PTFE strip and the Al foil strip. Figure S4 shows the output current of the FS-TENG with the strip width of 1−2 cm and length of 15−27 cm at frequency 4 Hz. Figure S5 shows the output current and voltage comparison of the FS-TENGs with and without ICP reactive-ion etching, from which we can see that the surface modification of the PTFE films greatly enlarges the output performance.

The output performance of the FS-TENG depends on the coupling of friction and electrostatic induction, which is strongly affected by the contact/separation distance and strength of friction. Therefore, we choose three different deformation amplitudes to compare in the experiment. The peak output current increases from 4.87 to 34.7 μA as the deformation amplitude rises from 1.5 to 2.5 cm with the strip width and length of 3 and 21 cm at deformation frequency of 4 Hz (Figure 4c). Figure 4d presents the photographs at different

DOI: 10.1021/acsami.5b06675
ACS Appl. Mater. Interfaces 2015, 7, 20469−20476

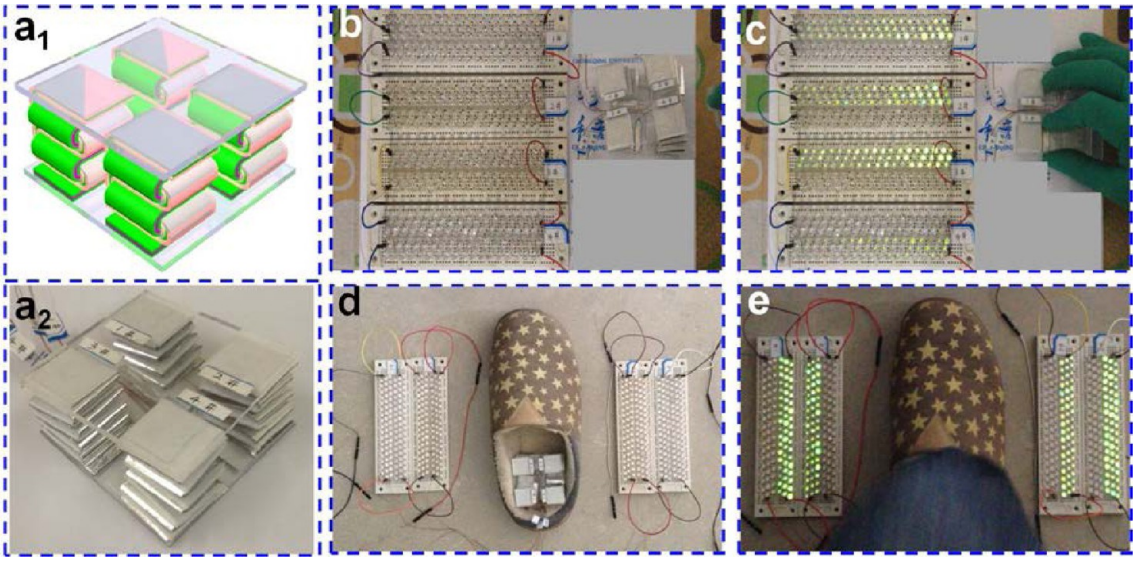

Figure 6. Schematic diagram (a_1) and digital photograph (a_2) of the SFS-TENG. The digital photographs of the SFS-TENG connected with four LED arrays (b), the working process under human hand flap (c), a slipper with a SFS-TENG located in the heel part (d), and the working process under human walking (e).

deformation amplitudes, where the natural length of the FS-TENG without pressure is about 5.5 cm (Figure 4d_1), and the deformation amplitude (A) reaches 2 and 2.5 cm, respectively (Figure 4d_2,d_3). When the deformation amplitude A is small, only a few of the PTFE segments and Al segments contact, and the PTFE segments do not fully contact Al segments, which results in low output current. As the amplitude increases, more surfaces contact each other tightly, which leads to more induced charges and charge transfer thereby enlarging the output current. Figure S6 displays the output currents of the FS-TENGs with lengths of 15 and 27 cm and width of 3 cm at 4 Hz.

Figure 4e shows a three-dimensional surface map smoothed by bilinear difference arithmetic, which displays the overall relationships between the output current and the strip length and deformation frequency. The output current obviously increases as the strip length and the deformation frequency increase. Similarly, the dependence of the output current on both the deformation amplitude and the deformation frequency in Figure 4f presents a similar variation trend as that in Figure 4e.

As for the TENGs, the output power with different external loads is an important standard to evaluate their practical value. Figure 4g shows the dependence of the output current and open-circuit voltage on the external loading resistance. As the resistance increases, the output current gradually decreases, while the open-circuit voltage reveals an opposite trend, increasing from ∼0.007 V at 100 Ω to 840 V at 720 MΩ. The output power of the FS-TENG reaches the maximum of 7.33 mW at external loading resistance of 20 MΩ. The output power density is about 626 mW/m^2. The detailed calculations are shown in Supporting Information (page S-17).

For a single FS-TENG, the height changes with the weight or pressure on the top due to its spring structure. On the basis of this property, the FS-TENG can be used as a weight sensor. Figure 5a illustrates the digital photographs of the compressed FS-TENG under different weights and their output current signals. As can be seen from Figure 5a_1, the PTFE segments hardly contact the Al electrode segments with a weight of 10 g. Accordingly, its output signal is very weak. As the weight increases, contact friction surfaces begin to increase, and full contact is achieved when the weight reaches 100 g. The output signals increase correspondingly. Figure 5b shows the schematic diagram of the weight sensor. Figure 5c indicates that the output current increases with an increase in weight, which approximately complies with a liner function. The output currents under weights 50 and 100 g are about 3 and 5 μA, as are shown in Figure 5d_1,d_2, respectively. We also evaluate the sensitivity of the weight sensor with different lengths and pressure,[26] as is shown in Figure S7. The sensitivity S is defined as $S = (\Delta I/I_{off})/\Delta P$, where ΔI, I_{off}, and ΔP are the relative change in current, the current of the weight sensor without pressure, and the applied pressure, respectively. The similar curves of the three sensors with different lengths indicate reliable to evaluate the weight. Video 1 exhibits the working process of the weight sensor in Supporting Information.

To broaden the application of the FS-TENG, we have integrated four single FS-TENGs to fabricate a sandwiched FS-TENG (SFS-TENG). Figure 6a_1,a_2 shows the schematic diagram and photograph of the SFS-TENG. In order to reduce the total size of the TENG, four FS-TENGs with strip width of 2 cm are chosen and placed on the corners of the acrylic plates. The total size of the SFS-TENG is 6 cm × 6 cm × 3 cm. This SFS-TENG can harvest the mechanical energy of flapping hands and walking steps. As can been seen in Figure 6b, four single FS-TENGs are, respectively, connected with four light-emitting dioxide (LED) arrays, which are connected in series. When one's hand flaps on the top plate, four FS-TENGs work together and generate four output currents to power the corresponding LED arrays in Figure 6c (see video 2 in Supporting Information), demonstrating the effective electric output. The SFS-TENG can also be put into the heel part of a shoe to harvest the motion energy of human walking, as is depicted in Figure 6d. The electric energy generated by harvesting walking steps can light up the LED arrays, as is shown in Figure 6e (See video 3 and video 4 in Supporting Information). Since a flexible capacitor or battery can be

DOI: 10.1021/acsami.5b06675
ACS Appl. Mater. Interfaces 2015, 7, 20469−20476

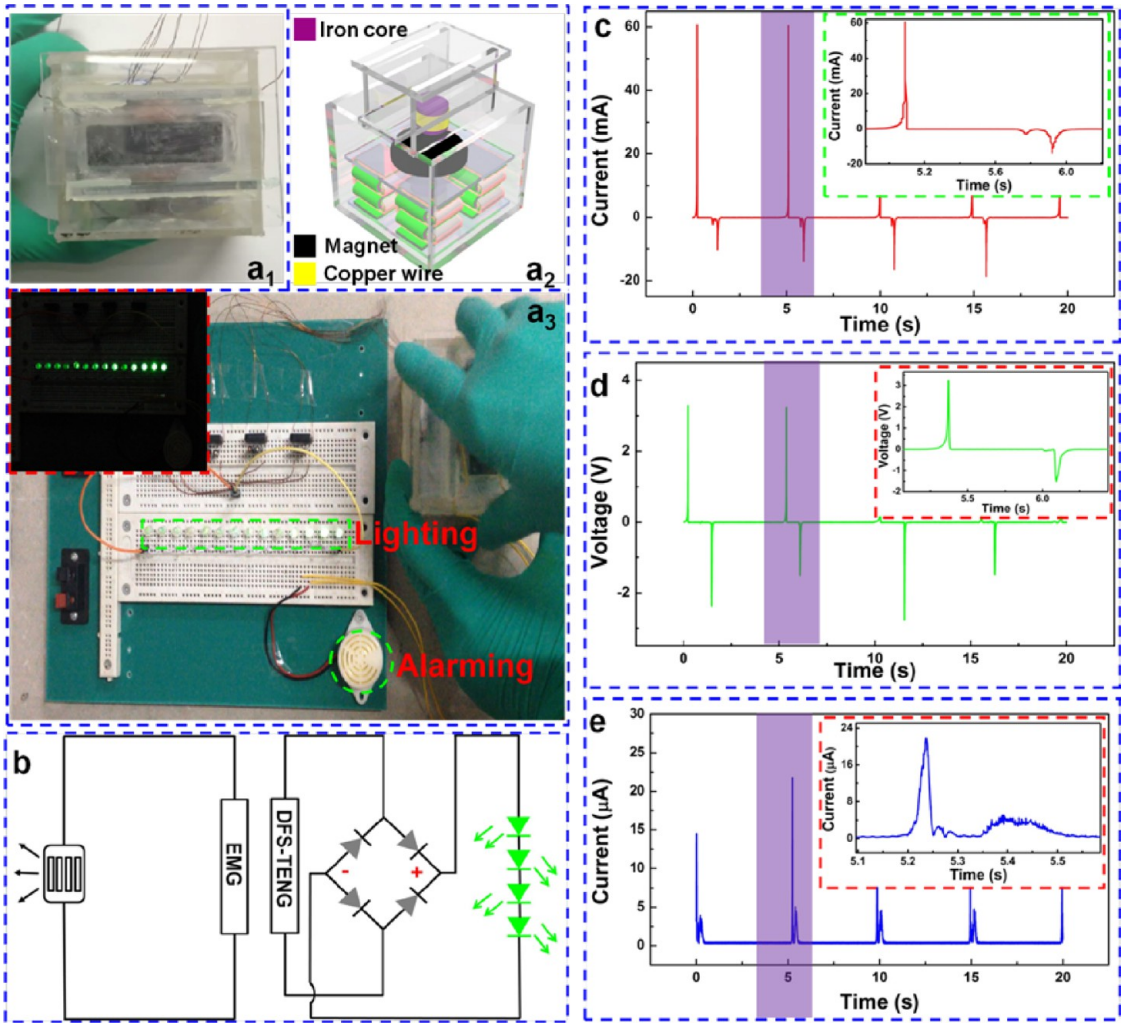

Figure 7. Digital photograph and schematic diagram of the DFS-TENG (a_1, a_2) and the setup and working process of the DFS-TENG (a_3). The equivalent circuit of the DFS-TENG (b). The output current (c) and open-circuit voltage (d) of the EMG. The output current of the SFS-TENG after rectification (e). The insets are the enlarged image of the selected peaks.

installed into an upper part of shoes, the IFS-TENG provides a wearable electric source.

Self-power is a desired mode for mobile electronic devices in the future. One advantage of a TENG is that it can harvest energy from the ambient and convert it into electricity to power the devices without any external power source. To achieve a self-driven device, a doorbell based on the FS-TENG (DFS-TENG) is fabricated. Figure 7a_1,a_2 illustrates the digital photograph and schematic diagram of the DFS-TENG, which mainly consists of a SFS-TENG and an electromagnetic generator (EMG). A plate supported by two vertical acrylic plates fixed on the movable part of FS-TENG works as a "button" of doorbell. Figure S8 shows the fabrications and structures of the components. In this experiment, the EMG is used to increase the output performance of the DFS-TENG. When the "button" is pressed, the TENG shrinks, and the permanent magnet is separated from the copper coil, which generates an electromagnetic induced current. The output currents of four FS-TENGs are rectified and added together. Afterward, the combined current of the FS-TENGs is used to light 14 green LEDs, which work as signal lamps. The EMG is directly used to drive the buzzer bell to alarm. The parameters of the buzzer bell are in Figure S9 in Supporting Information. As one presses the "button", the magnet separates from the coil and generates an induced current in the copper coil, and then the buzzer bell connected between the two ends of the coil begins to alarm. The output electricity of the FS-TENGs can light up the signal lamps and drive the buzzer bell to work simultaneously, as is shown in Figure 7a_3. The working flowchart, experiment setup and process of the self-powered doorbell are presented in Figures S10 and S11and video 5. Figure 7b shows the equivalent circuit of the DFS-TENG. The output current and open-circuit voltage of the EMG reach 55 mA and 3.5 V, respectively (Figure 7c,d), while the output current of the TENG reaches up to 25 μA after the rectification (Figure 7e). The enlarged current and voltage signals in one cycle are shown in the insets. The triboelectric voltage of the device is shown in Figure S12 in Supporting Information. From the above, it demonstrates that the DFS-TENG can be applied in self-driven doorbell system.

Due to the specific structure of the FS-TENG, we fabricate a box FS-TENG (BFS-TENG) consisting of 12 single FS-TENG units with two balls in the center to realize more functions. Figure 8a,b illustrates the photograph and schematic diagram of the BFS-TENG. Two balls knock the IFS-TENG to make all the FS-TENG units work well simultaneously by an applied

DOI: 10.1021/acsami.5b06675
ACS Appl. Mater. Interfaces 2015, 7, 20469−20476

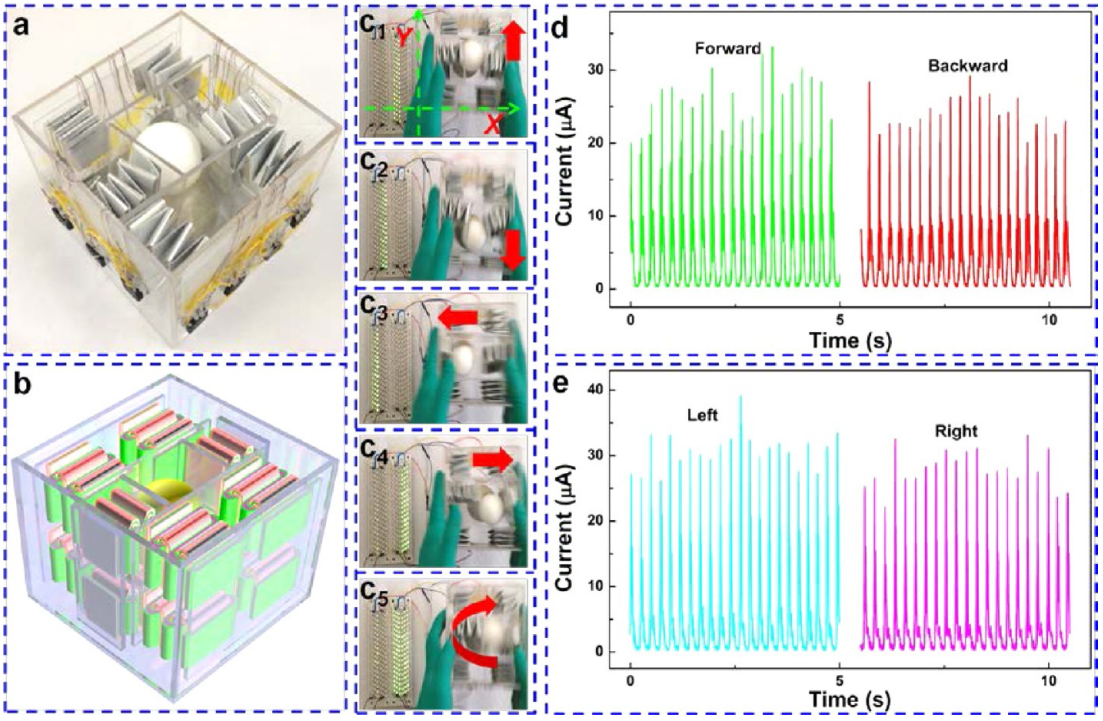

Figure 8. Digital photograph (a) and schematic diagram of the BFS-TENG (b). The working processes under different waggling directions (c). The output currents when waggled forward and backward (d), left and right (e), respectively.

force. The output current from all the single FS-TENG units is rectified and is added together by being connected in series. Figure S13 shows the schematic diagram of the connection among the FS-TENGs in the BFS-TENG. When the box waggles forward and backward under the external force, the balls move forward and backward to knock the IFS-TENGs, generating two output current signals, which light up two LED arrays (Figure 8c_1,c_2). When the box moves left and right, two IFS-TENGs standing opposite are pressed by the balls, which also generates two output currents (Figure 8c_3,c_4). Furthermore, the BFS-TENG can also work in rotary mode and knock the four IFS-TENGs alternately. The output current of the BFS-TENG working in forward/backward and right/left is shown in Figure 8d,e, respectively. Video 6 in Supporting Information shows the detailed working process of the BFS-TENG. The produced electricity can be stored in a capacitor or a Li-battery, which can power other miniaturized devices like cell phones and electronic watches.

4. CONCLUSIONS

In summary, we have designed and fabricated a folded elastic strip-based triboelectric nanogenerator (FS-TENG). The output electricity of the FS-TENG increases with an increase in the strip width and length, deformation frequency, and amplitude. The output current, open-circuit voltage, and peak power reach up to 55 μA, 840 V, and 7.33 mW (0.626 W/m^2), respectively, for the FS-TENG with the strip width of 3 cm and length of 27 cm at the deformation frequency of 4 Hz with the amplitude of 2.5 cm. Due to its good elasticity, the FS-TENG can be used as a weight sensor to detect different weights. An integrated generator assembled by four FS-TENGs (IFS-TENG) can harvest the energy of human motion like palm flapping and footsteps. In addition, the IFS-TENG combined with electromagnetic induced electricity can achieve a completely self-driven doorbell that produces an alarm by a buzzer and flashing signal by lights. When four IFS-TENGs are installed into an acrylic box (BFS-TENG), it can work in translational and spin motions, which can harvest energy in all directions. This work promotes the research on completely self-driven systems and energy harvesting of human motion for multiple applications in our daily life.

■ ASSOCIATED CONTENT

Supporting Information

The Supporting Information is available free of charge on the ACS Publications website at DOI: 10.1021/acsami.5b06675.

Figures S1−S13, description of surface modification and corrosion procedures, and calculation of power density (PDF)

Video showing working process of the weight sensor (AVI)

Video of four FS-TENGs working together (AVI)

Video of LED arrays lighting up though walking energy with FS-TENGs inside the shoe (AVI)

Video of LED arrays lighting up through walking energy with FS-TENGs outside the shoe (AVI)

Video showing working process of the self-powered doorbell (AVI)

Video showing working process of the box FS-TENG (AVI)

■ AUTHOR INFORMATION

Corresponding Author

*Phone: +86 23 65620880. Fax: +86 23 65678362. E-mail: hucg@cqu.edu.cn.

Notes

The authors declare no competing financial interest.

DOI: 10.1021/acsami.5b06675
ACS Appl. Mater. Interfaces 2015, 7, 20469−20476

■ ACKNOWLEDGMENTS

This work is supported by the National High Technology Research and Development Program (863 program) of China (2015AA034801), NSFC (51572040, 11204388), the Fundamental Research Funds for the Central Universities (CQDXWL-2014-001 and CQDXWL-2013-012), and the large-scale equipment sharing fund of Chongqing University.

■ REFERENCES

(1) Jung, J. H.; Lee, M.; Hong, J.; Ding, Y.; Chen, C. Y.; Chou, L. J.; Wang, Z. L. Lead-free $NaNbO_3$ Nanowires for a High Output Piezoelectric Nanogenerator. *ACS Nano* **2011**, *5*, 10041−10046.

(2) Shin, S. H.; Kim, Y. H.; Lee, M. H.; Jung, J. Y.; Nah, J. Hemispherically Aggregated BaTiO3 Nanoparticle Composite Thin Film for High-Performance Flexible Piezoelectric Nanogenerator. *ACS Nano* **2014**, *8*, 2766−2773.

(3) Lee, K. Y.; Kim, D.; Lee, J. H.; Kim, T. Y.; Gupta, M. K.; Kim, S. W. Unidirectional High-power Generation via Stress-Induced Dipole Alignment from ZnSnO3 Nanocubes/Polymer Hybrid Piezoelectric Nanogenerator. *Adv. Funct. Mater.* **2014**, *24*, 37−43.

(4) Leng, Q.; Chen, L.; Guo, H. Y.; Liu, J. L.; Liu, G. L.; Hu, C. G.; Xi, Y. Harvesting Heat Energy from Hot/Cold Water with a Pyroelectric Generator. *J. Mater. Chem. A* **2014**, *2*, 11940−11947.

(5) Yang, Y.; Wang, S. H.; Zhang, Y.; Wang, Z. L. Pyroelectric Nanogenerators for Driving Wireless Sensors. *Nano Lett.* **2012**, *12*, 6408−6413.

(6) Yang, Y.; Jung, J. H.; Yun, B. K.; Zhang, F.; Pradel, K. C.; Guo, W. X.; Wang, Z. L. Flexible Pyroelectric Nanogenerators Using a Composite of Lead-Free KNbO3 Nanowires. *Adv. Mater.* **2012**, *24*, 5357−5362.

(7) Fan, F. R.; Lin, L.; Zhu, G.; Wu, W. Z.; Zhang, R.; Wang, Z. L. Transparent Triboelectric Nanogenerators and Self-Powered Pressure Sensors Based on Micropatterned Plastic Films. *Nano Lett.* **2012**, *12*, 3109−3114.

(8) Fan, F. R.; Tian, Z. Q.; Wang, Z. L. Flexible Triboelectric Generator. *Nano Energy* **2012**, *1*, 328−334.

(9) Kanik, M.; Say, M. G.; Daglar, B.; Yavuz, A. F.; Dolas, M. H.; El-Ashry, M.; Bayindir, M. A Motion- and Sound-Activated, 3D-Printed, Chalcogenide-Based Triboelectric Nanogenerator. *Adv. Mater.* **2015**, *27*, 2367−2376.

(10) Guo, H. Y.; Leng, Q.; He, X. M.; Wang, M. J.; Chen, J.; Hu, C. G.; Xi, Y. A Triboelectric Generator Based on Checker-like Interdigital Electrodes with a Sandwiched PET Thin Film for Harvesting Sliding Energy in all Directions. *Adv. Energy Mater.* **2015**, *5*, 1400790.

(11) Yang, W. Q.; Chen, J.; Zhu, G.; Wen, X. N.; Bai, P.; Su, Y. J.; Lin, Y.; Wang, Z. L. Harvesting Vibration Energy by a Triple-Cantilever Based Triboelectric Nanogenerato. *Nano Res.* **2013**, *6*, 880−886.

(12) Tang, W.; Han, C. B.; Zhang, C.; Wang, Z. L. Cover-sheet-based Nanogenerator for Charging Mobile Electronics Using Low-Frequency Body Motion/Vibration. *Nano Energy* **2014**, *9*, 121−127.

(13) Xie, Y. N.; Wang, S. H.; Niu, S. M.; Lin, L.; Jing, Q. S.; Su, Y. J.; Wu, Z. Y.; Wang, Z. L. Multi-Layered Disk Triboelectric Nanogenerator for Harvesting Hydropower. *Nano Energy* **2014**, *6*, 129−136.

(14) Guo, H. Y.; Chen, J.; Yeh, M.-H.; Fan, X.; Wen, Z.; Li, Z. L.; Hu, C. G.; Wang, Z. L. An Ultrarobust High-Performance Triboelectric Nanogenerator Based on Charge Replenishment. *ACS Nano* **2015**, *9*, 5577−5584.

(15) Yang, W. Q.; Chen, J.; Zhu, G.; Yang, J.; Bai, P.; Su, Y. J.; Jing, Q. S.; Cao, X.; Wang, Z. L. Harvesting Energy from the Natural Vibration of Human Walking. *ACS Nano* **2013**, *7*, 11317−11324.

(16) Bai, P.; Zhu, G.; Lin, Z. H.; Jing, Q. S.; Chen, J.; Zhang, G.; Ma, J. S.; Wang, Z. L. Integrated Multilayered Triboelectric Nanogenerator for Harvesting Biomechanical Energy from Human Motions. *ACS Nano* **2013**, *7*, 3713−3719.

(17) Sun, C.; Shi, J.; Bayerl, D. J.; Wang, X. D. PVDF Microbelts for Harvesting Energy from Respiration. *Energy Environ. Sci.* **2011**, *4*, 4508−4512.

(18) Guo, H. Y.; Chen, J.; Tian, L.; Leng, Q.; Xi, Y.; Hu, C. G. Airflow-induced Triboelectric Nanogenerator as a Self-Powered Sensor for Detecting Humidity and Airflow Rate. *ACS Appl. Mater. Interfaces* **2014**, *6*, 17184−17189.

(19) Zhu, W.; Wu, Y. Y.; Wang, C. Y.; Zhang, M.; Dong, G. X. Fabrication of Large-Area 3D Ordered Silver-Coated Colloidal Crystals and Macroporous Silver Films Using Polystyrene Templates. *Nano-Micro Lett.* **2013**, *5*, 182−190.

(20) Seung, W.; Gupta, M. K.; Lee, K. Y.; Shin, K. S.; Lee, J. H.; Kim, T. Y.; Kim, S.; Lin, J. J.; Kim, J. H.; Kim, S. W. Nanopatterned Textile-Based Wearable Triboelectric Nanogenerator. *ACS Nano* **2015**, *9*, 3501−3509.

(21) Chen, J.; Zhu, G.; Yang, W. Q.; Jing, Q. S.; Bai, P.; Yang, Y.; Hou, T. C.; Wang, Z. L. Harmonic-resonator-Based Triboelectric Nanogenerator as a Sustainable Power Source and a Self-Powered Active Vibration Sensor. *Adv. Mater.* **2013**, *25*, 6094−6099.

(22) Jeong, C. K.; Baek, K. M.; Niu, S. M.; Nam, T. W.; Hur, Y. H.; Park, D. Y.; Hwang, G. T.; Byun, M.; Wang, Z. L.; Jung, Y. S.; Lee, K. J. Topographically-Designed Triboelectric Nanogenerator via Block Copolymer Self-Assembly. *Nano Lett.* **2014**, *14*, 7031−7038.

(23) Zhou, T.; Zhang, C.; Han, C. B.; Fan, F. R.; Tang, W.; Wang, Z. L. Woven Structured Triboelectric Nanogenerator for Wearable Devices. *ACS Appl. Mater. Interfaces* **2014**, *6*, 14695−14701.

(24) Guo, H. Y.; Chen, J.; Leng, Q.; Xi, Y.; Wang, M. J.; He, X. M.; Hu, C. G. Spiral-Interdigital-Electrode-Based Multifunctional Device: Dual-Functional Triboelectric Generator and Dual-Functional Self-Powered Sensor. *Nano Energy* **2015**, *12*, 626−635.

(25) Meng, X. S.; Li, H. Y.; Zhu, G.; Wang, Z. L. Fully Enclosed Bearing-Structured Self-Powered Rotation Sensor Based on Electrification at Rolling Interfaces for Multi-Tasking Motion Measurement. *Nano Energy* **2015**, *12*, 606−611.

(26) Yang, P. K.; Lin, Z. H.; Pradel, K. C.; Lin, L.; Li, X. H.; Wen, X. N.; He, J. H.; Wang, Z. L. Paper-Based Origami Triboelectric Nanogenerators and Self-Powered Pressure Sensors. *ACS Nano* **2015**, *9*, 901−907.

(27) Wang, Z. L. Triboelectric Nanogenerators as New Energy Technology for Self-Powered Systems and as Active Mechanical and Chemical Sensors. *ACS Nano* **2013**, *7*, 9533−9557.

(28) Zhu, G.; Chen, J.; Zhang, T. J.; Jing, Q. S.; Wang, Z. L. Radial-Arrayed Rotary Electrification for High Performance Triboelectric Generator. *Nat. Commun.* **2014**, *5*, 3426.

DOI: 10.1021/acsami.5b06675
ACS Appl. Mater. Interfaces 2015, 7, 20469−20476